Microwave photonic-assisted analog-to-digital converters using quantum dash mode-locked laser

Xie, Yuxuan; Liu, Guocheng; Liu, Jiaren; Lu, Zhenguo; Poole, Philip J.; Zhao, Ping; Barrios, Pedro; Chen, Lawrence R.

Publisher’s version / Version de l'éditeur:

https://doi.org/10.1109/JLT.2025.3586999

Journal of Lightwave Technology, pp. 1-8, 2025-07-08

Microwave Photonic-assisted Analog-to-digital Converters Using Quantum Dash Mode-locked Laser

Yuxuan Xie *Student Member, IEEE*, Guocheng Liu, Jiaren Liu, Zhenguo Lu, *Senior Member, IEEE* , Philip J. Poole, Ping Zhao, Pedro Barrios, and Lawrence R. Chen, *Senior Member, IEEE*

***Abstract*— This paper introduces two photonic analog-to-digital converters (ADCs) for RF and millimeter wave (mmWave) signal processing. The time-interleaved photonic ADC uses optical taps to increase the sampling rate, while the heterodyne photonic ADC down-converts input signals to intermediate frequencies (IF) in the optical domain, optimizing bandwidth and sampling. Both achieve an effect number of bits (ENOB) of 6 to 11 and support high-frequency signals, including IEEE V-band, as well as complex modulations. Moreover, these two photonic ADCs share the same programmable and reconfigurable microwave photonic (MWP) system setup with the only modification being a change in the length of optical fiber used.**

***Index Terms*— Microwave photonics, Analog to digital conversion, Quantum dash laser,**

I. INTRODUCTION

Analog-to-digital converters (ADCs) are crucial components in modern electronic systems, enabling the translation of real-world analog signals into digital data that can be processed, stored, and analyzed by digital systems. As the demand for higher data rates and improved signal processing capabilities grows, traditional electronic ADCs face limitations in terms of speed, bandwidth, and power consumption [1,2]. Especially, the problem of timing jitter of the clock is a bottleneck in conventional ADCs [3]. To overcome these challenges, photonic ADCs are a promising alternative, leveraging the unique properties of light to achieve superior performance. Photonic ADCs utilize optical components and techniques to perform the conversion from analog to digital. By exploiting the high speed and wide bandwidth of photonic systems, these converters can achieve faster sampling rates and handle higher-frequency signals compared to their electronic counterparts. These characteristics make photonic ADCs ideal for applications in communications, radar, and signal processing where performance and efficiency are paramount. Traditionally, detection systems have used oscilloscopes with digital signal processing (DSP), but limitations in the sampling frequency of ADCs complicate direct detection. Consequently, conventional methods have employed RF/mmWave mixers, which are restricted to operational bandwidths of tens of GHz [4,5] and require a local oscillator (LO) for down-conversion. Given the formidable task of designing LOs for extremely high frequencies, often referred to as the THz gap [6], conventional solutions struggle to transcend this upper limit. The microwave photonics (MWP)-based photonic ADC systems offer broad bandwidths due to the high operational frequencies of electro-optical modulators (EOMs) and photodiodes (PDs), reaching hundreds of GHz [7,8].

Several methods exist for implementing photonic ADC systems, with many leveraging an optical frequency comb (OFC) source [2,9]. The photonic sampled ADC completes the sampling process in the optical domain by modulating the input signal on an optical pulse train [10–14]. However, the detection of the sampled pulse train cannot be directly detected, and devices such as high-speed optical switches [10–12] and wavelength division demultiplexers [13,14], are required. The time-stretch photonic ADC reduces the bandwidth requirement of the PD by modulating an RF signal onto a chirped Gaussian pulse, subsequently expanding the modulated signal through a dispersive medium [15–17]. Nevertheless, the modulation format suggests that the sampled signal will exhibit a chirped Gaussian envelope, introducing additional distortion and requiring post-DSP for recovery. The time-interleaved photonic ADC, whose principle is the same as an equivalent-time (or relative-time) sampling oscilloscope, implements the time-interleaving process in the optical domain. Like a sampling oscilloscope, the time-interleaved photonic ADC only works for periodic signals. However, it can also be effectively used for eye diagram analysis of real data signals. Completing the time-interleaving process requires a uniform time delay between optical taps, which can be achieved through, e.g., a multi-core fiber with a tunable laser [1]. However, the total number of taps is constrained by the number of cores in such fibers. Another solution involves utilizing an OFC source and a linear dispersive medium, such as optical fiber. OFC-based solutions can provide more taps than multi-core fibers. Moreover, an increased number of taps can reduce the clock frequency requirements prior to time-interleaving, potentially enabling the sampling unit to operate below the Nyquist rate. The last type of photonic ADC involves optical heterodyne detection [18]. By modulating the input signal onto an optical carrier and beating it with an optical local oscillator (LO), the input signal is down-converted into an intermediate frequency (IF), which can then be easily detected by a conventional ADC. However, the optical carrier and LO must meet three requirements to ensure the accuracy of detection:

Manuscript received on DD MM 2024; revised DD MM 2024; accepted DD MM 2024. Date of publication DD MM 2024; date of current version DD MM 2024. (Corresponding author: Yuxuan Xie, yuxuan.xie@mail.mcgill.ca)

Yuxuan Xie and Lawrence R. Chen are with Department of Electrical and Computer Engineering, McGill University, Montreal, Quebec, Canada.

Guocheng Liu, Jiaren Liu, Zhenguo Lu, Philip J. Poole, Ping Zhao, and Pedro Barrios are with Advanced Electronics and Photonics Research Center, National Research Council Canada, Ottawa, Ontario, Canada

Color versions of one or more of the figures in this article are available online at http://ieeexplore.ieee.org

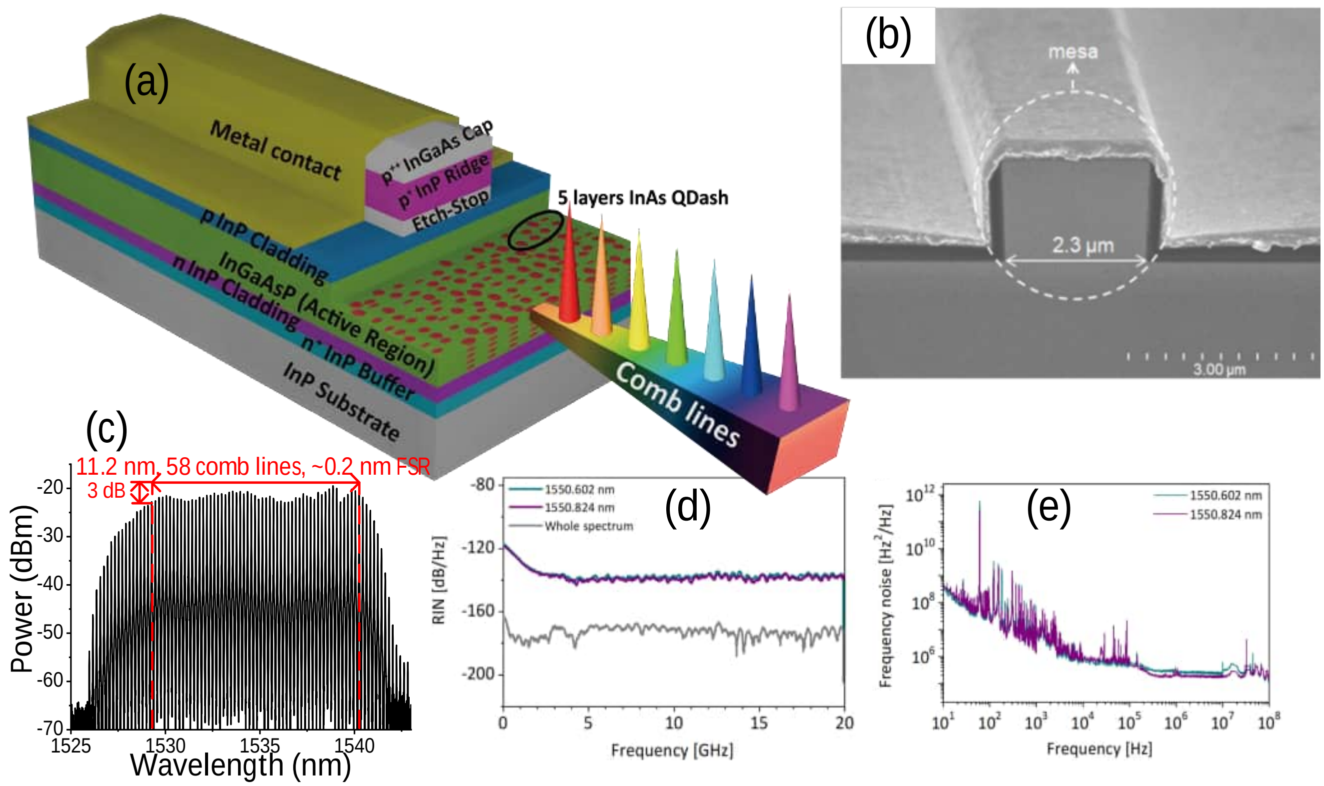

Fig. 1 (a) schematic of QDash laser, (b) scanning electron microscopy of the five InAs QDash layers, (c) the optical spectrum of QDash laser at 400 mA and 23 °C, (d) the RIN and (e) phase noise of the QDash laser [19].

1. contain minimal intensity noise,
2. exhibit constant and stable frequency spacing, and
3. be phase locked.

The first two conditions pose no challenge for a pair of continuous-wave (CW) lasers, widely used in optical coherent communications [20]. However, achieving the third condition, essential for recovering phase information without DSP, is unattainable with a pair of CW lasers [21]. Hence, an OFC source becomes necessary.

In this paper, we present a programmable and reconfigurable MWP system that can be used to implement two photonic ADCs, one time-interleaved and one heterodyne. The time-interleaved ADC boosts the sampling rate through optical tap interleaving, while the heterodyne ADC down-converts signals in the optical domain, optimizing bandwidth and ADC sampling. Both systems achieve an effect number of bits (ENOB) of 6 to 11, efficiently handle diverse waveforms and high-frequency signals, including IEEE V-band, and support real-time detection, proving their effectiveness for advanced communication systems.

II. Quantum Dash Mode-Locked Laser

The OFC source used in this paper is a quantum dash (QDash) mode-locked laser (MLL), whose layout is illustrated in Fig. 1 (a); Fig. 1 (b) is the scanning electron microscopy of the cross section. The active region comprises five stacked InAs QDash layers and lattice-matched $In_{0.816}Ga_{0.184}As_{0.392}P_{0.608}$ (1.15Q) barriers. Further details regarding the material growth of the QDash can be found in [22]. Utilizing a Fabry–Perot cavity, the output of the QDash laser is as a set of OFC lines with a free spectral range (FSR) of 25 GHz (~0.2 nm) in the C-band, as depicted in Fig. 1 (c). A noteworthy aspect of this MLL is its flat gain, yielding a quasi-flat comb spectrum over a 3-dB bandwidth of 11.2 nm. Additional details and discussions regarding the profiles of this QDash laser are available in [19,23,24].

For the time-interleaved photonic ADC, the phase performance of the QDash OFC source is not crucial; instead, a constant and stable FSR is required. After propagation through fiber, any instability in the FSR (drift) leads to non-uniform time delays, causing non-uniform interleaving. The maximum FSR drift of our QDash laser is less than ±50 kHz [19], which is negligible compared to its 25 GHz FSR. Additionally, a flat comb spectrum is mandatory for time-interleaved photonic ADCs, and this is a key feature of the QDash laser. In comparison to other non-flat OFC sources, such as micro-ring resonators [25], the comb shaping process is both easier and more energy efficient, because the comb lines do not need to be flattened relative to that having the lowest power. For the heterodyne photonic ADC, as the name suggests, the principle is based on optical heterodyne detection (or beating). Therefore, the OFC requirements are similar to those in optical coherent communications [20] and RF/mmWave over fiber systems [26–29]. Although the relative intensity noise (RIN) is just −132.1 dB/Hz across selected modes and −171.8 dB/Hz for the whole spectrum shown in Fig. 1 (d) [19], it does not really affect the MWP

This article has been accepted for publication in Journal of Lightwave Technology. This is the author's version which has not been fully edited and
content may change prior to final publication. Citation information: DOI 10.1109/JLT.2025.3586999

systems since the dominated amplitude noise in MWP systems is the amplified spontaneous emission (ASE) noise of optical amplifier. Instead, the phase noise characteristics are more important for photonic ADCs. As shown in Fig. 1 (e) whose frequency axis is normalized to the frequency of the beating tone (25 GHz), the QDash laser exhibits low phase noise and a narrow RF beating linewidth (mean value: 6.5 kHz). And the 1 ps wide full width at half-maximum (FWHM) suggests that all comb lines phase-locked [23]. The measured power drift across all comb lines is less than 0.1 dB, ensuring that both amplitude and phase information of the input signal are accurately recovered.

The motivation for using a QDash MLL as opposed to other OFC sources depends on the specific requirements of photonic ADCs discussed in this paper. Firstly, time-interleaved photonic ADCs demand as many flat comb lines as possible. In contrast, heterodyne photonic ADCs require only three comb lines but necessitate phase-locking characteristics. Among other OFC sources, ring-resonator-based OFC sources can generate flat comb spectra. While a well-controlled CW laser array or cascaded electro-optic modulator (EOM)-based OFC sources can also produce flat spectra, each comes with limitations. Achieving phase-locking with a CW laser array is highly challenging. Although cascaded EOM-based OFC sources can achieve phase-locking, they require a series of phase-locked RF/mmWave signal sources. In comparison, QDash MLL inherently satisfies all the critical requirements for both time-interleaved and heterodyne photonic ADCs, making it the optimal choice for the multifunctional photonic ADC applications demonstrated in this paper.

III. PRINCIPLES, RESULTS, AND DISCUSSION

A. System setup

Both the time-interleaved photonic ADC and the heterodyne photonic ADC can be implemented using the same experimental setup illustrated in Fig. 2. As a programmable and reconfigurable system, it can switch between the time-interleaved and heterodyne photonic ADC modes without major modifications. The 3 km SSMF (Corning SMF28, D=17ps/(km·nm)) and a tunable filter are arranged in parallel, and their selection is controlled by a pair of imaginary optical switches. Please note that the optical switches are imaginary because we simply replace the fiber by the filter in experiment. When both switches are set to the top position, the 3 km SSMF is connected, giving an approximate 10 ps delay for adjacent comb lines (i.e., with spacing of 0.2 nm) and enabling the system to operate as a time-interleaved photonic ADC. Conversely, when the switches are set to the bottom position, only the optical bandpass filter is connected, and the system functions as a heterodyne photonic ADC. Another difference between the time-interleaved and heterodyne photonic ADC setups lies in the comb shaping, controlled by the waveshaper (Finisar WS 16000, a programmable optical filter). For heterodyne ADC, the role of the waveshaper is limited to selecting three comb lines and compensating for the power differences among them. For time-interleaved photonic ADC, the waveshaper first compensates for the flatness error within the 3 dB flatness region, and then sequentially sweeps across the entire spectrum to isolate one comb line during each sweep.

The waveforms under test are generated by an arbitrary waveform generator (AWG, Keysight M9502A) while the sampling process is completed using a real-time oscilloscope (Tektronix DPO73304SX). Finally, it is important to note that all the results presented in this paper are DSP-free, i.e., no adaptive algorithms nor equalization are used to recover the received signal. Only some simple lowpass and bandpass filter are applied.

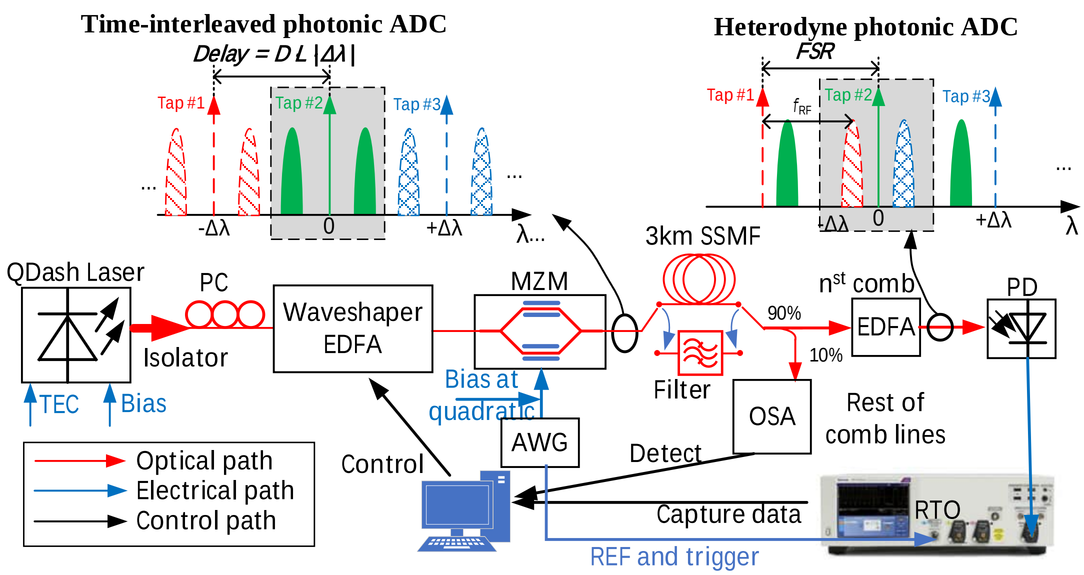

Fig. 2 Experimental setup of photonic ADCs. QDash: quantum dash laser, TEC: thermoelectric cooler, PC: polarization controller, MZM: Mach-Zehnder modulator, SSMF: standard single mode fiber, EDFA: Erbium-doped fiber amplifier, OSA: optical spectrum analyzer, AWG: arbitrary waveform generator and RTO: real-time oscilloscope

This article has been accepted for publication in Journal of Lightwave Technology. This is the author's version which has not been fully edited and content may change prior to final publication. Citation information: DOI 10.1109/JLT.2025.3586999

B. Time-interleaved photonic ADC

This section discusses our time-interleaved photonic ADC, whose principle is the same as a sampling oscilloscope. Therefore, all waveforms used in this section are periodic, and they are not detected in real-time. Fig. 3 illustrates the time-interleaving principle using two comb lines. After modulating the comb lines with the sinusoid, the two waveforms (red and black traces or dots) are overlapped as in Fig. 3 (a). Then, after propagating through the 3 km SSMF, the waveform of one comb line is shifted by 10 ps relative to the other, see Fig. 3 (b). Please note that there is an artificial amplitude shift between the red and black lines in Fig. 3 (b) to show them separately and clearly. Once the arbitrary amplitude shift is removed, time-interleaving is very clear, i.e., each red dot is located exactly in the middle of two adjacent black dots, as illustrated in Fig. 3 (c). All operations above are completed by controlling all equipment with MATLAB automatically. With such high efficiency operation, more complex waveform can be demonstrated.

Next, we evaluate the effect number of bits (ENOB) of this photonic ADC. By sweeping with a standard sinusoid, the ENOB of our photonic ADC is shown in Fig. 4 (a) with different clock frequencies, where their equivalent sampling rates are the same. Please note that the original sampling frequency of all signals in Fig. 4 (a) is 50 GHz, and different sampling frequencies are obtained by down-sampling. The ENOB is calculated based on:

$$= \frac{-\ 1.76}{6.02} \qquad (1)$$

Note: $6.02 \approx 20 \cdot {}_{10}(2), 1.76 \approx 10 \cdot {}_{10}(3/2)$

where the signal-to-noise and distortion ratio (SINAD) is calculated in MATLAB based on the power spectral density of the recovered signal. The best ENOB we achieved is 11. The ENOB here is limited by the white noise in the optical system since our system is DSP free. In each line, the sampling frequency is constant. Hence, an increase in frequency of the input signal leads to a decrease in the over-sampling ratio. Therefore, the ENOB decreases as the frequency increases.

Although the results in Fig. 3 and Fig. 4 (a) demonstrate the functionality of our system with standard sinusoids, verifying its efficacy with arbitrary signals is imperative. We now use more complex waveforms to demonstrate further the capability of our system. Also, the time-interleaved ADC only needs to ensure that the sampling frequency after interleaving (called equivalent sampling frequency later) meets the Nyquist sampling theory, which suggests that the clock frequency can be lower than the Nyquist frequency. Some results in Fig. 4 (a) already show that, but they are obtained based on down-sampling. To enhance the persuasiveness of our results, we physically set the clock frequency of the RTO at 3.125 GHz (50/16, where 50 GHz is the fundamental frequency) and use 32 comb lines for time-interleaving. The waveform under test this time is a 4 GHz asymmetric sinusoid (see the red reference in Fig. 4 (b)). With an RTO sampling frequency of 3.125 GS/s, all samples before time-interleaving suffer distortion because of aliasing, as plotted in the black square marks in Fig. 4 (b). Nevertheless, with the help of the 32 comb lines, a time-interleaved waveform sampled at 100 GS/s can be still recovered, as illustrated in Fig. 4 (c). This result proves that even if the signal already suffers aliasing while sampling, the photonic ADC can still recover the original waveform.

The signals demonstrated in Fig. 3 and Fig. 4 are all discrete in the frequency domain. In telecommunications, all applied signals are continuous in the frequency domain. Hence, we continue to test an even more complex waveform, and in particular one where the frequency spectrum is not discrete, such as a chirped sinusoid. Here, the waveform under test is a chirped sinusoid with center frequency 3 GHz. In Fig. 5 (a), we first capture the chirped sinusoid with a 50 GHz sampling frequency. Then, down-sampling to 2 GS/s is applied to the captured signal. After interleaving with 50 comb lines, the signal is recovered with an equivalent sampling frequency of 100 GS/s. The frequency of the input signal linearly varies from 1 to 5 GHz repeatedly, as shown in Fig. 5 (c and d). Fig. 5 (c) presents the chirp spectrogram of the reference signal (red dashed line in Fig. 5 (a and b)), and Fig. 5 (d) shows the case with black dots. Finally, we physically set the sampling frequency to 3.125 GS/s to demonstrate that the photonic ADC can still function correctly. The results are shown in Fig. 5 (b and e). Please note that the reference signal in Fig. 5 (b) is obtained from Fig. 5 (a) and manually aligned with the signal because the original reference in Fig. 5 (b) already suffered distortion.

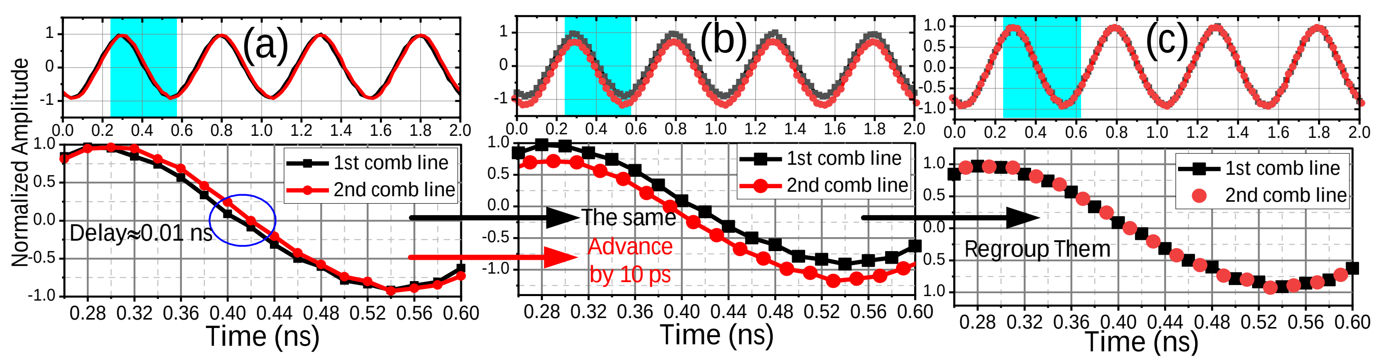

Fig. 3 A demonstration of the principle of time-interleaving process. (a) raw data before time-interleaving, (b) during the time-interleaving, and (c) after time-interleaving process.

This article has been accepted for publication in Journal of Lightwave Technology. This is the author's version which has not been fully edited and content may change prior to final publication. Citation information: DOI 10.1109/JLT.2025.3586999

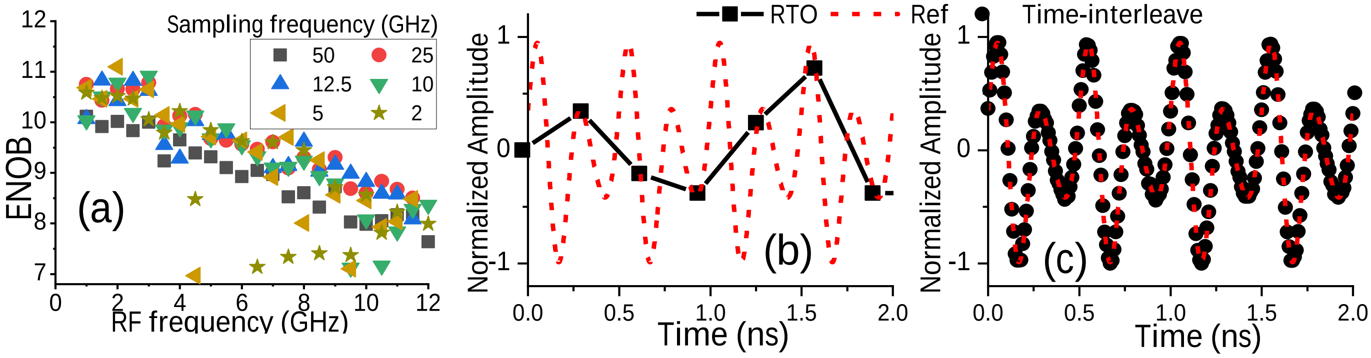

Fig. 4 Experiment results of photonic time-interleaved ADC for (a) ENOB of time-interleaved photonic ADC, (b) a 4 GHz asymmetric sinusoid sampled at 3.125 GHz and (c) the same asymmetric sinusoid after time-interleaving.

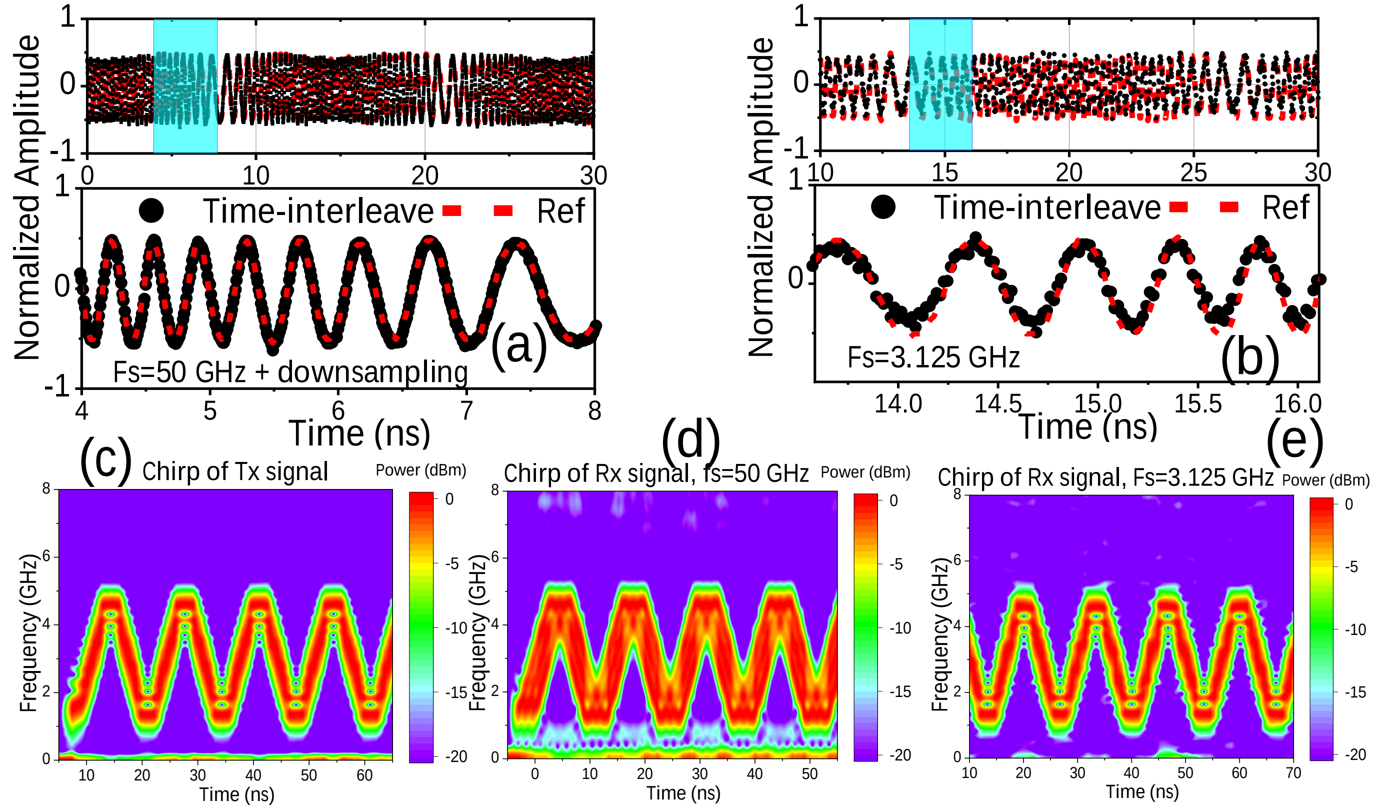

Fig. 5 Experiment results of photonic time-interleaved ADC for chirped sinusoid (a) detected with 50 GHz sampling frequency and down-sampling, (b) detected with sampling frequency 3.125 GHz, (c-e) chirp analyzes for all signals in (a and b).

C. Heterodyne photonic ADC

The motivation of heterodyne photonic ADC is reducing the requirement of the bandwidth of the PD and the clock frequency of the sampling unit. The time-interleaved photonic ADC can only reduce the requirement of the sampling frequency. But the heterodyne photonic ADC can improve both. The principle of the heterodyne photonic is plotted at the top right of Fig. 2. Usually in conventional MWP systems, the maximum input RF frequency should be lower than half of the FSR to prevent cross-talk between taps [28]. However, the heterodyne photonic ADC diverges from this convention; instead, we make use of the cross-talk. As depicted in the top-right corner of Fig. 2, after modulating the RF signal onto the taps, the sideband of each tap is located near its neighboring taps. Consequently, if we solely detect the frequency components near the central taps (highlighted in grey), which are isolated by an optical bandpass filter, the input RF signal will be down-converted into an IF signal whose frequency is determined by

$$= | \quad - \quad \cdot \quad |, \quad \geq 1 \qquad (2)$$

where f_{IN} is the frequency of the input signal, N is an integer. In this paper, we only discuss the case when $N=1$. The significance of is in isolating one comb line from every comb lines using the waveshaper. This selection is predicated

This article has been accepted for publication in Journal of Lightwave Technology. This is the author's version which has not been fully edited and content may change prior to final publication. Citation information: DOI 10.1109/JLT.2025.3586999

on ensuring that the input frequency and satisfy the following condition:

$$0.5 \cdot \quad \cdot \quad < \quad < 0.5 \cdot (\quad + 2) \cdot \qquad (3)$$

Hence, for signals within the 5G New Radio (NR) band, N=1 is the optimal choice. Moreover, for higher frequency signals, such as THz signals, our system exhibits potential for down-conversion, given that the maximum N in our system can reach 58/3≈19, where 58 is the total number of flat comb lines of the QDash laser, and the heterodyne photonic ADC requires 3 comb lines.

During the experiment, the RF/mmWave signal is generated by an AWG with a maximum output frequency of 32 GHz. To showcase the state-of-art of our photonic ADC, which obviates the need for a wide-bandwidth PD, we introduce a 7.5 GHz low-pass filter to restrict the bandwidth of the PD. The output signal is directly captured by a RTO. Notably, there is no synchronization between the RTO and AWG, and no DSP is applied for optimization. The aim is to demonstrate the real-time capability of the system without relying on DSP.

We initially evaluate the performance of our heterodyne photonic ADC using the ENOB. According to Eq. (2), there are two scenarios to consider: when the input frequency is either greater than or less than the FSR (25 GHz). The ENOB is measured using a tunable frequency sinusoidal input from 18 to 32 GHz, and the results are depicted in Fig. 6 (a). In this figure, the reference is obtained by directly connecting the AWG and the RTO, with the frequency sweep based on the down-converted frequency (i.e., f_{IF} in Eq. (2)). For input frequencies below 25 GHz, the ENOB of our photonic ADC closely matches the reference, indicating that the ENOB is limited by the performance of the AWG and RTO. However, for RF frequencies exceeding 25 GHz, the ENOB degrades. This degradation is attributable to the input frequency approaching the maximum bandwidth of our MZM. Additionally, the Nyquist sampling theory is applicable only to the received signal frequency(f_{IF}). This indicates that the ADC's sampling rate can be lower than the Nyquist rate of the input signal. To validate this concept, we varied the RTO's sampling rate from 100 GS/s to 12.5 GS/s, with the results presented in Fig. 6 (b). This figure illustrates the case where the input frequency is below 25 GHz. The maximum ENOB achieved was 11. Remarkably, even with a sampling rate of only 12.5 GS/s, our system maintained an ENOB greater than 5 while detecting signals in the 18-24 GHz range.

The ENOB results in Fig. 6 are all based on sinusoidal inputs. To demonstrate the applicability of our system for 5G communication signals, results with complex signals are required. Unlike the time-interleaved photonic ADC, the heterodyne photonic ADC can support real-time detection. In other words, no trigger is required, enabling us to directly process telecommunication signals. Here, we utilized the photonic ADC to detect a 23 GHz signal with a 1 GHz bandwidth for various modulation formats, including on-off keying (OOK), 4-level pulse-amplitude modulation (PAM4), and binary phase-shift keying (BPSK). The results are presented in Fig. 7. Due to the limitation of space, we only show eye-diagrams here, and more details including time-domain waveforms, spectra, and eye-diagrams with different sampling frequency are available in Supplementary Materials. Please note that all Q factors in this paper are unitless (not dB scale). In each set of results, we first show the time domain waveforms of the received (down-converted) signals, with highlight marks on all 4-power levels of PAM4 signals and the phase shift of π for BPSK signals. Next, the electrical spectra of the transmitted (Tx) and received (Rx) signals are illustrated. Due to the beating between the three comb lines, the Tx signal at 23 GHz is down-converted to 2 GHz. Benefiting from the stability of the FSR as well as the good phase noise performance, and the received eye diagram does not exhibit significant timing jitter nor phase error. Finally, since the frequency of the received signal is just 2 GHz, it is possible to reduce the sampling frequency from 100 GS/s to 12.5 GS/s (for OOK) or 25 GHz (for BPSK and PAM4) without indicates any distortion, and there is only a <1.5 penalty in the Q factor.

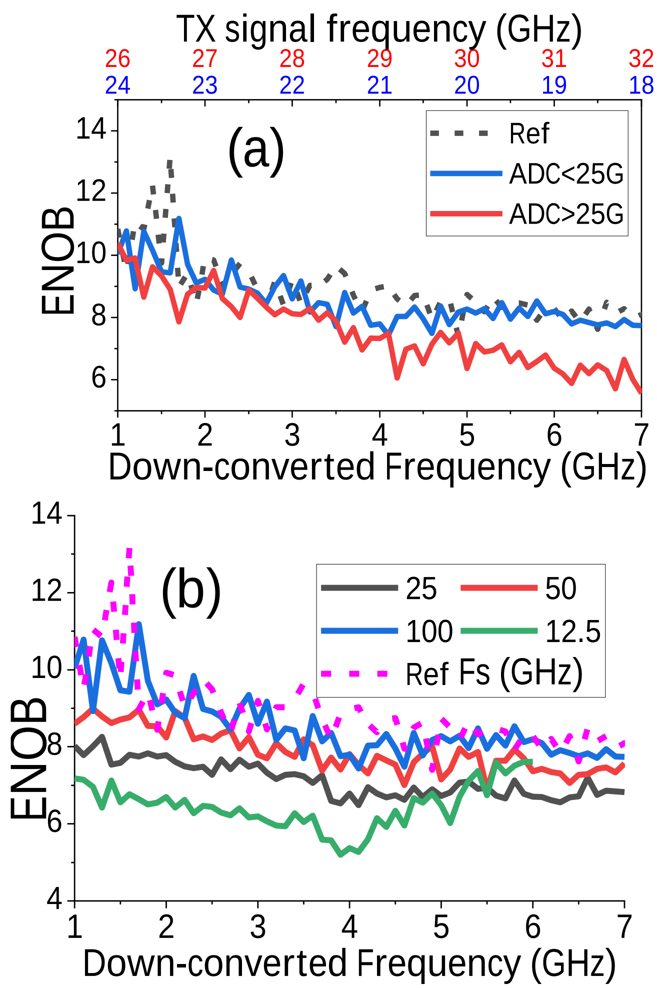

Fig. 6 Experimental results of (a) ENOB of the heterodyne photonic ADC with different input frequencies, where the sampling frequency is 100 GS/s. (b) ENOB of the photonic ADC with different sampling frequency where the x-axis is the down-converted frequency.

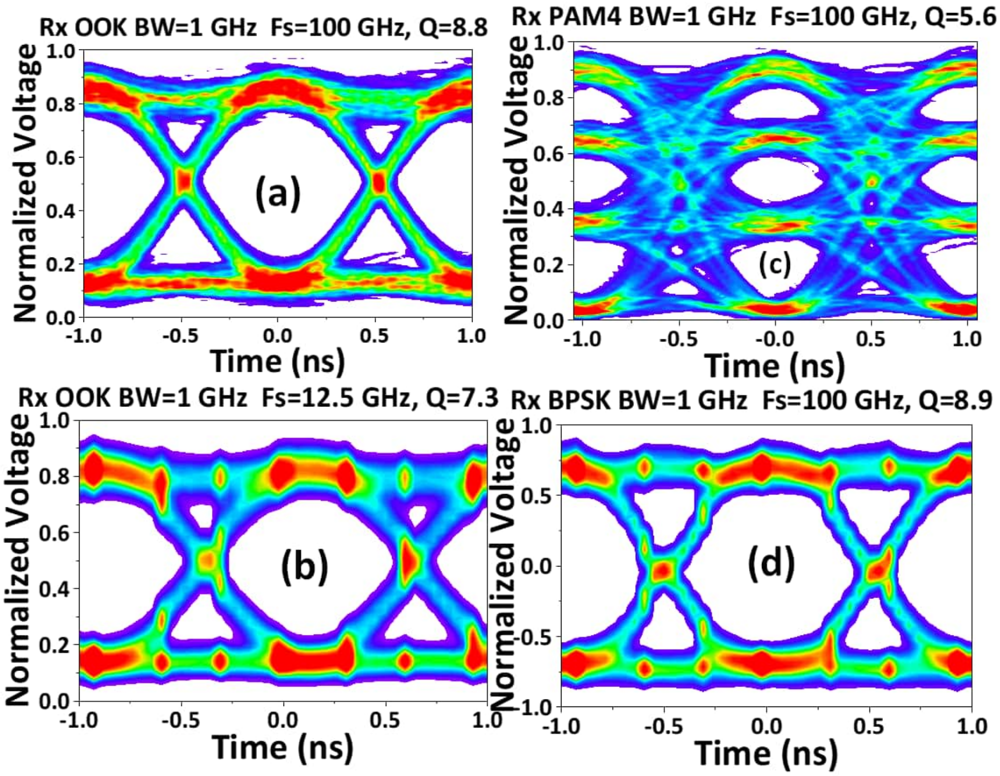

Fig. 7 (a) Received eye-diagram of a 23 GHz, 1 GHz bandwidth OOK signal, (b) the same signal as (a) but detected with sampling frequency of 12.5 GHz. (c) received eye-diagram of a 23 GHz, 1 GHz bandwidth PAM4 signal, and (d) received eye-diagram of a 23 GHz, 1 GHz bandwidth BPSK signal. The sampling frequency of (a, c and d) is 100 GS/s

D. Discussion and future work

Both photonic ADCs can significantly reduce the clock frequency requirement of the sampling unit, with the sampling frequency even falling below the Nyquist rate of the input signal. The heterodyne photonic ADC is specifically designed for the demodulation of RF/mmWave signals and supports real-time detection. However, it cannot recover the original signal's frequency, as the detected signal has been down-converted. On the other hand, the time-interleaved photonic ADC can recover the original frequency, but the results are relative to time. Additionally, the bandwidth requirements of the time-interleaved photonic ADC are higher than those of the heterodyne photonic ADC. Fortunately, the programmability of the MWP system allows for switching between time-interleaved and heterodyne photonic ADC modes to adapt to different situations. Finally, the heterodyne photonic ADC has demonstrated its capability to detect a 1 GHz bandwidth mmWave signal, indicating its potential application for 5G OFDM signal detection. This idea has been validated through simulations using OptiSystem, and experimental implementation is planned in our future work.

IV. Conclusion

This paper presents two photonic ADCs designed for RF and mmWave signals. The time-interleaved photonic ADC multiplies the equivalent sampling rate by interleaving with optical taps, enabling operation with clock frequencies below the Nyquist rate. The heterodyne photonic ADC optimizes the bandwidth requirements of the PD and the sampling frequency of the ADC by down-converting the input signal into an IF signal in the optical domain. These two photonic ADCs achieve an ENOB ranging from 6 to 11 across the operating frequency range. They perform well with various waveforms, and the heterodyne photonic ADC even supports real-time detection. Additionally, these photonic ADCs have the potential to detect higher frequency signals, such as those in the IEEE V-band, and to accommodate more complex modulation formats, indicating their applicability in modern communication systems. Furthermore, these two photonic ADCs are implemented using the 58 flat and phase-locked comb lines generated by the QDash MLL. In the time-interleaved photonic ADC, the input RF signal must be duplicated across all comb lines, necessitating a flat comb spectrum. The large number of comb lines significantly reduces the clock frequency requirements of the sampling unit. At the same time, the phase-locking characteristics of the OFC lines enable the heterodyne photonic ADC to operate without the need for DSP. Additionally, the extensive number of comb lines allows the system to achieve higher operational frequencies in the future. Since the QDash laser satisfies all the critical requirements, these two photonic ADCs can be implemented in the same setup, and the length of the fiber is the only modification to switch functions. The successful implementation and testing of these photonic ADCs highlight their feasibility and effectiveness for advanced signal processing applications. Their capability to handle high-frequency signals and complex modulation schemes makes them promising candidates for integration into future 5G and beyond communication systems. Further research and development could enhance their performance and broaden their range of applications, solidifying their role in the evolution of photonic signal processing technologies.

ACKNOWLEDGMENT

This research was supported by the National Research Council Canada under projects HTSN-206 and HTSN-245 and by the Natural Sciences and Engineering Research Council of Canada. The authors would also like to acknowledge Canadian Photonics Fabrication Center (CPFC) and Advanced Technology Fabrication (ATF) of the Advanced Electronics and Photonics (AEP) Research Centre at the National Research Council Canada for the material growth and device fabrication.

REFERENCES

[1] S. García, M. Ureña, and I. Gasulla, "Photonic-Assisted Analog-to-Digital Conversion Based on a Dispersion-Diversity Multicore Fiber," *IEEE J. Select. Topics Quantum Electron.*, vol. 29, no. 6: Photonic Signal Processing, pp. 1–8, Nov. 2023, doi: 10.1109/JSTQE.2023.3267507.

[2] G. C. Valley, "Photonic Analog-to-Digital Converters," *Opt. Express, OE*, vol. 15, no. 5, pp. 1955–1982, Mar. 2007, doi: 10.1364/OE.15.001955.

[3] A. Khilo *et al.*, "Photonic ADC: Overcoming the Bottleneck of Electronic Jitter," *Opt. Express*, vol. 20, no. 4, p. 4454, Feb. 2012, doi: 10.1364/OE.20.004454.

[4] S. Lee *et al.*, "28-GHz CMOS Up-Conversion Mixer With Improved LO Second-Harmonic Leakage Signal Suppression for 5G Applications," *IEEE Access*, vol. 10, pp. 57003–57011, 2022, doi: 10.1109/ACCESS.2022.3178440.

[5] B. Bae *et al.*, "24–40 GHz Dual-Band Highly Linear CMOS Up-Conversion Mixer for mmWave 5G NR FR2 Cellular Applications," *IEEE Microw. Wireless Compon. Lett.*, vol. 32, no. 8, pp. 999–1002, Aug. 2022, doi: 10.1109/LMWC.2022.3161092.

[6] D. R. Gulevich, V. P. Koshelets, and F. V. Kusmartsev, "Bridging the Terahertz Gap for Chaotic Sources with Superconducting Junctions," *Phys. Rev. B*, vol. 99, no. 6, p. 060501, Feb. 2019, doi: 10.1103/PhysRevB.99.060501.

[7] E. Abacıoğlu *et al.*, "500 GHz Operational Bandwidth MUTC-Photodiodes with Milliwatt Terahertz Output Power Levels," in *49th European Conference on Optical Communications (ECOC 2023)*, Hybrid Conference, Glasgow, UK: Institution of Engineering and Technology, 2023, pp. 1410–1413. doi: 10.1049/icp.2023.2572.

[8] M. Burla *et al.*, "500 GHz Plasmonic Mach-Zehnder Modulator Enabling Sub-THz Microwave Photonics," *APL Photonics*, vol. 4, no. 5, p. 056106, May 2019, doi: 10.1063/1.5086868.

[9] P. T. Callahan, M. L. Dennis, and T. R. C. Jr, "Photonic Analog-to-Digital Conversion," *JOHNS HOPKINS APL TECHNICAL DIGEST*, vol. 30, no. 4, 2012.

[10] X. Zhu, D. Zhu, and S. Pan, "A Photonic Analog-to-Digital Converter with Multiplied Sampling Rate Using a Fiber Ring," in *2017 International Topical Meeting on Microwave Photonics (MWP)*, Oct. 2017, pp. 1–3. doi: 10.1109/MWP.2017.8168671.

[11] L. Pierno *et al.*, "Optical Switching Matrix as Time Domain Demultiplexer in Photonic ADC," in *2013 European Microwave Integrated Circuit Conference*, Oct. 2013, pp. 41–44. Accessed: Apr. 18, 2024. [Online]. Available: https://ieeexplore.ieee.org/abstract/document/6687780

[12] H. Gevorgyan, K. Al Qubaisi, M. S. Dahlem, and A. Khilo, "Silicon Photonic Time-Wavelength Pulse Interleaver for Photonic Analog-to-Digital Converters," *Opt. Express*, vol. 24, no. 12, p. 13489, Jun. 2016, doi: 10.1364/OE.24.013489.

[13] T. R. Clark, J. U. Kang, and R. D. Esman, "Performance of a Time- and Wavelength-Interleaved Photonic Sampler for Analog-Digital Conversion," *IEEE Photonics Technology Letters*, vol. 11, no. 9, pp. 1168–1170, Sep. 1999, doi: 10.1109/68.784241.

[14] J. Olson, D. S. Perlmutter, P. T. S. DeVore, and J. T. Chou, "Real-Time Jitter Correction in a Photonic Analog-to-Digital Converter," *Opt. Lett.*, vol. 45, no. 18, p. 5089, Sep. 2020, doi: 10.1364/OL.397249.

[15] A. Fard, B. Buckley, and B. Jalali, "Spectral Efficiency Improvement in Photonic Time-Stretch Analog-to-Digital Converter via Polarization Multiplexing," *IEEE Photon. Technol. Lett.*, vol. 23, no. 14, pp. 947–949, Jul. 2011, doi: 10.1109/LPT.2011.2142414.

[16] F. Coppinger, A. S. Bhushan, and B. Jalali, "Photonic Time Stretch and Its Application to Analog-to-Digital Conversion," *IEEE Trans. Microwave Theory Techn.*, vol. 47, no. 7, pp. 1309–1314, Jul. 1999, doi: 10.1109/22.775471.

[17] Y. Zhang *et al.*, "Broadband Transient Waveform Digitizer Based on Photonic Time Stretch," *J. Lightwave Technol.*, vol. 39, no. 9, pp. 2880–2887, May 2021, doi: 10.1109/JLT.2021.3061511.

[18] I. Morohashi *et al.*, "High Precision Frequency Measurement of Terahertz Waves Using Optical Combs from a Mach–Zehnder-Modulator-Based Flat Comb Generator," *Opt. Lett.*, vol. 44, no. 3, p. 487, Feb. 2019, doi: 10.1364/OL.44.000487.

[19] G. Liu *et al.*, "Monolithic InAs/InP Quantum Dash Mode-Locked Lasers for Millimeter-Wave-Over-Fiber Mobile Fronthaul Systems," *IEEE J. Select. Topics Quantum Electron.*, vol. 29, no. 6: Photonic Signal Processing, pp. 1–10, Nov. 2023, doi: 10.1109/JSTQE.2023.3273539.

[20] M. Khalil *et al.*, "Performance of Quantum-Dash Mode-Locked Lasers (QD-MLLDs) for High-Capacity Coherent Optical Communications," *Opt. Express*, vol. 32, no. 1, p. 217, Jan. 2024, doi: 10.1364/OE.509643.

[21] X. Liu *et al.*, "Thin-Film Lithium Niobate-Based Electro-Optic Comb Cloning for Self-Homodyne Coherent Communication," *Opt. Lett.*, vol. 49, no. 11, p. 3238, Jun. 2024, doi: 10.1364/OL.527403.

[22] P. J. Poole, K. Kaminska, P. Barrios, Z. Lu, and J. Liu, "Growth of InAs/InP-Based Quantum Dots for 1.55μm Laser Applications," *Journal of Crystal Growth*, vol. 311, no. 6, pp. 1482–1486, Mar. 2009, doi: 10.1016/j.jcrysgro.2009.01.129.

[23] G. Liu *et al.*, "Mode-Locking and Noise Characteristics of InAs/InP Quantum Dash/Dot Lasers," *J. Lightwave Technol.*, vol. 41, no. 13, pp. 4262–4270, Jul. 2023, doi: 10.1109/JLT.2023.3244777.

[24] Z. Lu *et al.*, "InAs/InP Quantum Dash Semiconductor Coherent Comb Lasers and Their Applications in Optical Networks," *J. Lightwave Technol.*, vol. 39, no. 12, pp. 3751–3760, Jun. 2021, doi: 10.1109/JLT.2020.3043284.

[25] X. Xu *et al.*, "Photonic Microwave True Time Delays for Phased Array Antennas Using a 49 GHz FSR Integrated Optical Micro-Comb Source [Invited]," *Photon. Res.*, vol. 6, no. 5, p. B30, May 2018, doi: 10.1364/PRJ.6.000B30.

[26] K. Zeb *et al.*, "Inas/Inp Quantum Dash Buried Heterostructure Mode-Locked Laser for High Capacity Fiber-Wireless Integrated 5g New Radio Fronthaul Systems," *Opt. Express*, vol. 29, no. 11, p. 16164, May 2021, doi: 10.1364/OE.424504.

[27] Z. Lu *et al.*, "Quantum Dot Coherent Comb Lasers for B5G/6G Mobile and Terrestrial Communication Systems," in *Integrated Optics: Devices, Materials, and Technologies XXVIII*, S. M. García-Blanco and P. Cheben, Eds., San Francisco, United States: SPIE, Mar. 2024, p. 37. doi: 10.1117/12.3000712.

[28] X. Xie *et al.*, "Bidirectional RoF 5G Fronthaul Transmission Links with an InAs/InP Quantum Dash Laser," in *2023 Photonics North (PN)*, Jun. 2023, pp. 1–1. doi: 10.1109/PN58661.2023.10222938.

[29] X. Xie *et al.*, "Frequency Multiplexing in Millimeter-Wave Over Fiber Fronthaul Transmission Links with an Inas/Inp Quantum Dash Mode-Locked Laser," in *Terahertz, RF, Millimeter, and Submillimeter-Wave Technology and Applications XVII*, L. P. Sadwick and T. Yang, Eds., San Francisco, United States: SPIE, Mar. 2024, p. 39. doi: 10.1117/12.3001643.